



Synthesis of Nanostructured Ni–TiO₂ Composite Coatings by Sol-Enhanced Electroplating

Weiwei Chen,^a Yedong He,^b and Wei Gao^{a,z}

^aDepartment of Chemical and Materials Engineering, The University of Auckland, Auckland 1142, New Zealand

^bBeijing Key Laboratory for Corrosion, Erosion and Surface Technology, University of Science and Technology Beijing, Beijing 100083, China

A Ni–TiO₂ composite film was prepared by electrodeposition containing Ti precursor sol (sol-enhanced deposition). The electrochemical process, microstructures, and properties of the sol-enhanced and traditional composite coatings were studied and compared. The sol-enhanced Ni–TiO₂ composite coating possessed a smooth surface and a compact microstructure and showed higher mechanical properties (430 HV₁₀₀) compared with the traditional coatings (360 HV₁₀₀). It is believed that the strengthening effects resulted from the high dispersion of TiO₂ nanoparticles. The sol added coatings also showed slower growth of Ni grains along the [220] direction but did not change the orientation. It is suggested that the sol addition reduced the thickness of the diffusion layer and increased the limited current density. Therefore, the polarization control in the sol-enhanced process changed from the traditional concentration polarization to electrochemical polarization, avoiding the formation of loose and dendritic structures at high current density.

© 2010 The Electrochemical Society. [DOI: 10.1149/1.3442366] All rights reserved.

Manuscript submitted March 22, 2010; revised manuscript received May 7, 2010. Published June 8, 2010.

Since the Watts solution was formulated in 1916, Ni electroplating has been a commercially important and versatile surface coating/finishing process.^{1,2} Ni or Ni alloys have been widely deposited on the surfaces of working parts to improve their corrosion and wear resistance or modify magnetic and other properties.²⁻⁴ To achieve better properties, the electrodeposited Ni or Ni alloys were modified by codepositing second-phase particles in the matrix called composite coatings. The traditional composite coating method is a solid particle mixing process: The second-phase particles are suspended in the Ni electroplating solution, and then both the particles and the Ni ions codeposit onto the specimens/parts to form composite coatings.⁴ The Ni-based composite coatings were fabricated earlier from suspensions of relatively large (typically micrometer level) particles of carbides,⁵ oxides,⁶ diamond,⁷ and Teflon.^{8,9} More recently, there has been increasing emphasis on codepositing Ni ions and superfine or nanosized particles to synthesize a new structure, i.e., nanocomposite coatings. The superfine/nanoparticles are dispersed into the Ni matrix, providing significantly improved properties, such as hardness and wear resistance.¹⁰⁻¹⁴

The strengthening mechanisms for nanocomposite coatings can be interpreted based on the dislocation model such as the Orowan theory.¹⁵ In this theory, the critical condition for a dislocation to bypass the particles in its glide plane is to bend the dislocation to a semicircle between the particles. The dislocation with its dipoles annihilated can move forward while dislocation loops are left behind, surrounding each particle.¹⁵⁻¹⁷ Orowan's criterion indicates that mechanical properties of composite coatings increase with both decreasing mean planar interparticle spacing and particle size.

Based on the above theory, the incorporation of second-phase superfine/nanoparticles can be much more effective than micro-sized particles in reinforcing the composite coatings. Theoretically, if the second-phase nanoparticles are highly dispersed in composite materials, the strong interaction between dislocation lines and the nanoparticles can almost completely block the movements of dislocations, leading to a huge improvement of mechanical properties.^{17,18} To achieve good dispersion of the nanoparticles, powder suspension has to be physically maintained in the solution by vigorous agitation, air injection, ultrasonic vibration, or adding surfactants. However, it is always difficult for nanoparticles to achieve good suspension because they have very large surface areas. The high surface energy tends to cause agglomeration of nanoparticles in composite coatings. Therefore, it has been a challenge to prepare highly dispersive nanoparticle reinforced composites or composite coatings.

The sol–gel process has been widely applied to prepare uniform nanosized particles.¹⁹⁻²⁴ Typically, the hydrolysis and condensation reactions take place in the sol–gel process to form metal oxides or their composite nanoparticles.^{25,26} The sol–gel process can be regarded as an in situ liquid phase synthesis of uniform nanoparticles at room temperature, providing a precursor to introduce nanoparticles into the composite electrodeposition. In the electroplating process, the metal ions discharge on the surface of the cathode through migration and diffusion in the electrolyte,⁴ which can provide an opportunity for the in situ formed nanoparticles to integrate immediately into the alloy deposit.

We have developed a novel nanostructured Ni–TiO₂ composite coating: sol-enhanced deposition by electroplating with a small amount of transparent TiO₂ sol in the electrolyte solution.^{27,28} This method led to a highly dispersive distribution of TiO₂ nanoparticles in the coating, avoiding the agglomeration of TiO₂ nanoparticles. The mechanical properties were therefore significantly improved. The present work is a systematic investigation of the electrochemical process of the sol-enhanced Ni–TiO₂ composite coating. The microstructures of the sol-enhanced and traditional composite coatings were closely compared and the electrochemical process involving the composite formation were discussed.

Experimental

Preparation of transparent TiO₂ sol.—According to the previous paper,^{27,29} 8.68 cm³ of tetrabutylorthotitanate [Ti(OBu)₄] was dissolved into the mixture solution of 35 cm³ ethanol and 2.82 cm³ diethanolamine (DEA). After magnetic stirring for 2 h, it was hydrolyzed by adding a mixture of 0.45 cm³ deionized water and 4.5 cm³ ethanol dropwise under magnetic stirring.

Electrodeposition of coatings.—Cylindrical medium carbon steels (0.50 wt % C) with a diameter of 15 mm and thickness of 3 mm were used as the substrates. Specimens were mechanically polished using SiC paper up to a grit of #1200 and then degreased ultrasonically in ethanol. Before electroplating, the specimens were pretreated in 1 mol dm⁻³ HCl solution for 2 min at room temperature. The bath composition and plating parameters used in the present work are listed in Table I. After 12.5 cm³ dm⁻³ TiO₂ sol was added into the bath, the electroplating was immediately conducted. At the same time, the solution was continuously magnetically stirred at a rate of 100 r min⁻¹. The traditional Ni and Ni–TiO₂ coatings were prepared with identical bath composition and plating parameters for comparison. The traditional Ni–TiO₂ composite coatings were prepared by using the solid particle mixing

^z E-mail: w.gao@auckland.ac.nz

Table I. The composition of electroplating bath and processing parameters.

Bath composition and processing parameters	Quantity
NiSO ₄ ·6H ₂ O	300 g dm ⁻³
NiCl ₂ ·6H ₂ O	45 g dm ⁻³
H ₃ BO ₃	40 g dm ⁻³
TiO ₂ sol	12.5 cm ³ dm ⁻³
Temperature	Room temperature
Current	10, 50, 100 mA cm ⁻²

method with a concentration of TiO₂ nanoparticles of 10 g dm⁻³. The TiO₂ powder (Sigma Co., Ltd.) has an anatase crystalline phase with an average diameter of <25 nm.

Characterization of coatings.— The content of TiO₂ particles in the composite coatings was calculated by the equation

$$C = \frac{\text{weight}(\text{TiO}_2)}{\text{weight}(\text{coating})} \times 100\% \quad [1]$$

The weight of TiO₂ particles in the composite coating was precisely measured by a chemical method described below. The Ni–TiO₂ composite coating was put into HNO₃ solution to be fully dissolved. TiO₂ particles do not react with HNO₃, so they precipitated out in the solution. The whole solution was set aside for 2 weeks to fully precipitate TiO₂ nanoparticles. Then the TiO₂ particles were separated with a centrifuge and calcined at 90°C for 20 h to remove the water. Finally, the dried TiO₂ particles were weighed using an electronic balance with an accuracy of 0.01 mg.

The coating morphologies were analyzed using a field-emission-scanning electron microscope. The phase structure of the coatings was determined using X-ray diffraction (XRD) with Cu K α radiation ($U = 40$ kV, $I = 40$ mA). Diffraction patterns were recorded in the 2θ range from 20 to 90° at a scanning rate of 0.02° s⁻¹. The

root-mean-square microstrain of the coatings was measured by the XRD line broadening analysis based on background subtraction and Ni lattice planes (111), (200), and (220). Microhardness of coatings was measured using a load of 100 g with a holding time of 15 s.

Results

Characterization of coatings.— Figure 1 shows the surface morphologies of Ni coatings and traditional and sol-enhanced Ni–TiO₂ nanocomposite coatings prepared at currents of 10, 50, and 100 mA cm⁻². The morphologies are quite different for the traditional and sol-enhanced composite coatings. The pyramid-like Ni nodules were formed on the surface of the traditional Ni plating at different currents (Fig. 1a1–a3). The size of the Ni nodules became larger when the current increased from 10 to 100 mA cm⁻². A dendritic surface formed when the Ni coating was prepared with a high current of 100 mA cm⁻² (Fig. 1a3). The incorporation of TiO₂ particles significantly changed the surface morphologies of the coatings. With the low current of 10 mA cm⁻², the spherical Ni nodules similarly exist on the surfaces of both traditional and sol-enhanced composite coatings but with different sizes (~500 nm in Fig. 1b1 and ~100 nm in Fig. 1c1). Obviously the sol-enhanced Ni–TiO₂ composite coating has a much smoother surface than the traditional counterpart.

However, for the traditional Ni–TiO₂ nanocomposite coating prepared at the current of 50 mA cm⁻², due to the fast growth of spherical Ni nodules, a cauliflower-like surface formed with the nodule size of ~5 μ m, on which many small nodules of ~500 nm in size can be seen (Fig. 1b2). In contrast, the fast growth of Ni nodules was largely inhibited for the sol-enhanced Ni–TiO₂ coatings, leading to the formation of a compact structure with fewer porosity and smoother surface (Fig. 1c2). The superfine Ni nodules (~400 nm) were distributed rather homogeneously on the surface, and the cauliflower-like structure disappeared (Fig. 1c2). The surface microstructure of the sol-enhanced composite coating was not changed much even at 100 mA cm⁻² (Fig. 1c2 and c3). For the

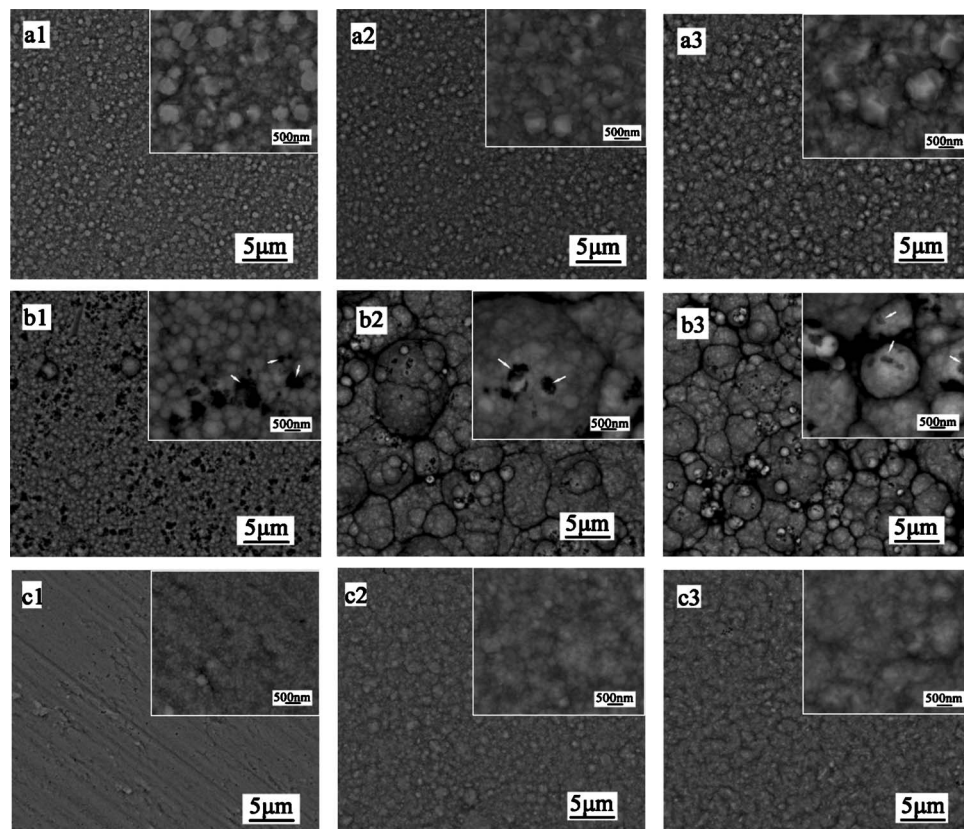


Figure 1. Surface morphologies of coatings: [(a1)–(a3)] Traditional Ni coatings, [(b1)–(b3)] traditional (solid powder mixing) Ni–TiO₂ nanocomposite coatings, and [(c1)–(c3)] sol-enhanced Ni–TiO₂ nanocomposite coatings. Each group of coatings was prepared at 10, 50, and 100 mA cm⁻².

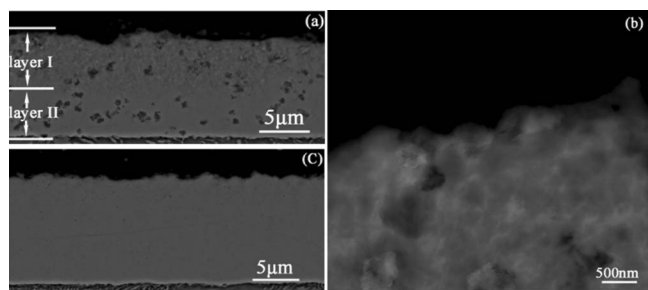


Figure 2. Cross-sectional morphologies of coatings prepared at 100 mA cm^{-2} : (a) The traditional Ni-TiO₂ composite coating showing a two-layer structure, (b) magnified image of layer I in (a), and (c) the sol-enhanced Ni-TiO₂ composite coating.

solid particle composite coating, with 100 mA cm^{-2} current density, the pillar-shaped nodules formed on the loose, dendritic surface (Fig. 1b3), a little similar to Ni coating (Fig. 1a3).

Large-scale clusters of nanosized TiO₂ particles are clearly seen on the surfaces of traditional Ni-TiO₂ composite coatings, as shown by the arrows in Fig. 1b3. In contrast, it is difficult to identify TiO₂ nanoparticles from the surface of the sol-enhanced composite coatings by the scanning electron microscopy images due to their small size and uniform distribution (Fig. 1c1-c3).

Figure 2 shows the cross-sectional morphologies of traditional and sol-enhanced Ni-TiO₂ composite coatings electroplated at 100 mA cm^{-2} . The traditional Ni-TiO₂ composite coating was divided into two layers with an outer loose layer (layer I) and an inner compact layer (layer II), as seen in Fig. 2a. Layer I indicated a dendritic structure (Fig. 2b), identical with the surface morphology in Fig. 1b3. In contrast, the sol-enhanced composite coating possessed a compact structure (Fig. 2c).

Figure 3 shows the content of TiO₂ nanoparticles in the traditional and sol-enhanced Ni-TiO₂ composite coatings. At 10 mA cm^{-2} , the traditional composite coating contains high TiO₂ ($\sim 4.3 \text{ wt } \%$). The contents of TiO₂ particles decreased when the traditional composite coatings were electrodeposited at higher currents. The sol-enhanced Ni-TiO₂ composite coating, however, contains lower TiO₂ particles ($\sim 3 \text{ wt } \%$ at 50 mA cm^{-2}) than traditional coatings. Similar contents ($\sim 1 \text{ wt } \%$) existed in both composite coatings when they were electrodeposited at the high current of 100 mA cm^{-2} .

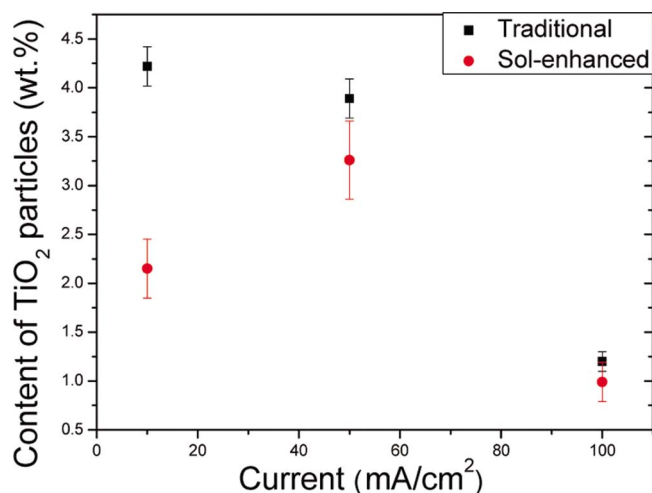


Figure 3. (Color online) The contents of TiO₂ nanoparticles in composite coatings prepared at 10, 50, and 100 mA cm^{-2} . (■: Traditional Ni-TiO₂ composite coating and red ●: Sol-enhanced Ni-TiO₂ composite coating.)

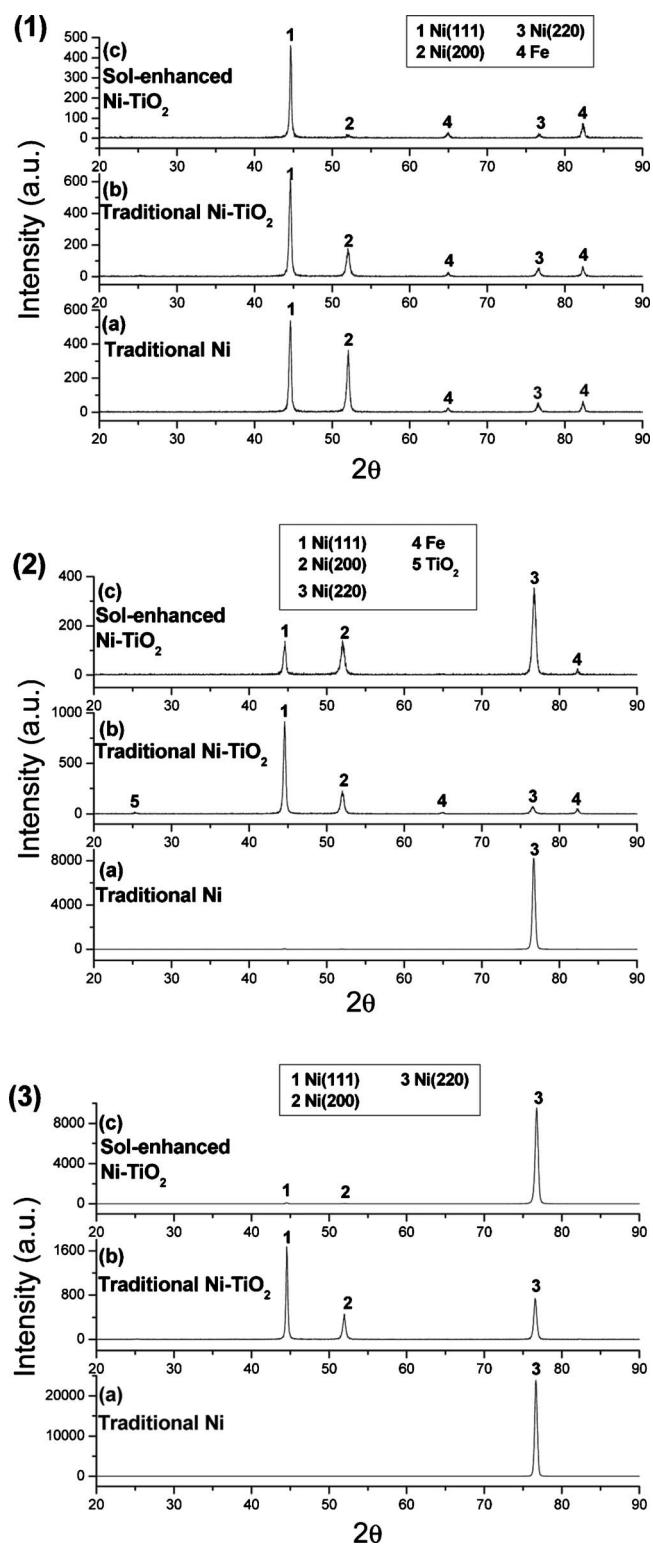


Figure 4. XRD patterns of the coatings prepared with the current of (1) 10, (2) 50, and (3) 100 mA cm^{-2} : (a) Traditional Ni coating, (b) traditional Ni-TiO₂ composite coating, and (c) sol-enhanced Ni-TiO₂ composite coating.

Phase structures.—Phase structures of traditional Ni coating and traditional and sol-enhanced Ni-TiO₂ composite coatings were analyzed by XRD, as shown in Fig. 4. At 10 mA cm^{-2} , the three coatings show similar phase structures with a preferential orientation

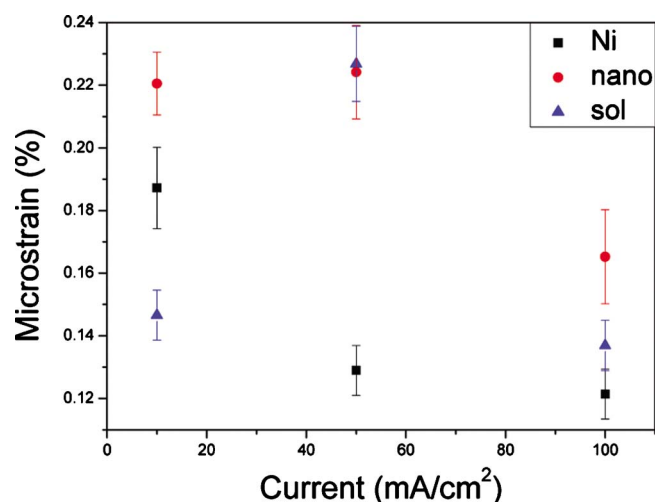


Figure 5. (Color online) The root-mean-square microstrain of different electroplating coatings prepared at 10, 50, and 100 mA cm⁻². (■: Traditional Ni coating, red ●: Traditional Ni–TiO₂ composite coating, and blue ▲: Sol-enhanced Ni–TiO₂ composite coating.)

along [111], indicating that the incorporation of TiO₂ particles does not have a significant effect on the phase structures.

The coatings electrodeposited at 50 and 100 mA cm⁻² have completely different phase structures. The phase structure is influenced by two factors, i.e., current and incorporation of TiO₂ nanoparticles. It can be seen from the XRD patterns of traditional Ni coatings that the orientation gradually changed from [111] to [220] when the current increased from 10 to 100 mA cm⁻², indicating that the high current density induced a preferential growth of Ni grains along [220]. However, with the incorporation of TiO₂ nanoparticles in the traditional composite coating, the growth of Ni grains along [220] is significantly reduced and, finally, the orientation of the coating shifted to [111] at 50 and 100 mA cm⁻². Similarly, the growth of Ni grains along [220] slowed down in the sol-enhanced Ni–TiO₂ composite coating process, but the orientation of the coating did not change, still along [220], in part reflecting the different influence mechanism of the sol-enhanced and particle-mixing methods. Meanwhile, a weak peak of TiO₂ was detected for the traditional Ni–TiO₂ composite coating prepared at 50 mA cm⁻².

Figure 5 shows the root-mean-square microstrain of the traditional Ni coating and the traditional and sol-enhanced Ni–TiO₂ composite coatings. It is widely accepted that the microstrain of composite coatings is mainly resulted from the lattice distortion due to the incorporation of second-phase particles. The same trend exists in both traditional and sol-enhanced Ni–TiO₂ composite coatings, i.e., the microstrain increases when the current increases, peaking at 50 mA cm⁻², and then declines. Both composite coatings have almost the same microstrain of ~0.22% when the coatings were electrodeposited at 50 mA cm⁻². In this case, as we have described previously, the TiO₂ nanoparticles (~4 wt %) agglomerated to form large clusters in the traditional Ni–TiO₂ composite coatings, compared to the highly dispersive distribution of TiO₂ nanoparticles in the sol-enhanced composite coating.²⁸ We propose that the strong lattice distortion occurred when the TiO₂ nanoparticles were highly dispersed in Ni matrix, leading to a large microstrain, although there was a smaller amount of nanoparticles (~3 wt %). At 100 mA cm⁻², the traditional composite coating possessed a higher microstrain than the sol-enhanced composite coating, although both coatings have a similar content of TiO₂ particles (Fig. 3). The higher microstrain is probably related to the dendritic structure in the traditional composite coating (Fig. 2a and b).

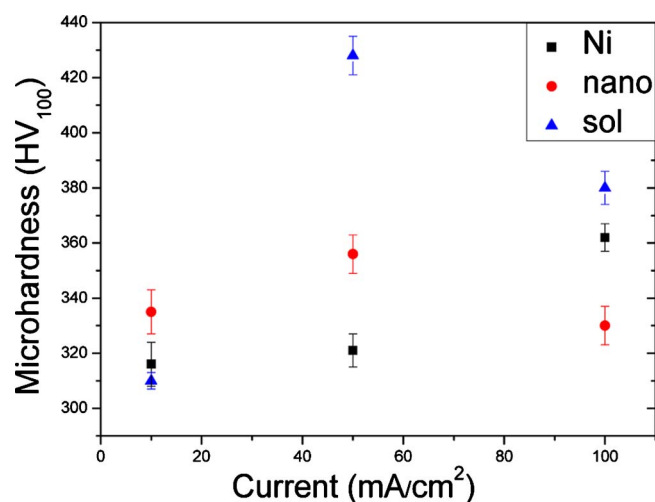


Figure 6. (Color online) Microhardness of the coatings prepared at 10, 50, and 100 mA cm⁻². (■: Traditional Ni coating, red ●: Traditional Ni–TiO₂ composite coating, and blue ▲: Sol-enhanced Ni–TiO₂ composite coating.)

Mechanical properties.—Figure 6 shows the microhardness of the traditional Ni coating and the traditional and sol-enhanced Ni–TiO₂ composite coatings prepared at 10, 50, and 100 mA cm⁻². The traditional and sol-enhanced Ni–TiO₂ composite coatings possess nearly the same trend in the current from 10 to 100 mA cm⁻². The highest microhardness: 430 HV₁₀₀ of the sol-enhanced coating formed at 50 mA cm⁻² was observed, corresponding to 20–34% improvement against ordinary Ni–TiO₂ composite (360 HV₁₀₀) and Ni plating (320 HV₁₀₀).

A strange result is that the traditional Ni–TiO₂ composite coating possesses a lower microhardness (~330 HV₁₀₀) than the Ni coating (~360 HV₁₀₀) when the coatings were prepared at the high current of 100 mA cm⁻². In contrast, the sol-enhanced Ni–TiO₂ composite coating has a higher microhardness of ~380 HV₁₀₀. Figure 6 shows that the microhardness of coatings is determined by both the incorporation of TiO₂ particles and processing parameters (current density), which affect the microstructure of coatings. As mentioned before, at 100 mA cm⁻², although the contents of TiO₂ particles are similar in both composite coatings (Fig. 3), the traditional Ni–TiO₂ composite coating showed a porous, dendritic surface (Fig. 1b3 and 2a and b), probably leading to the decrease in microhardness. In contrast, the compact structure in the sol-enhanced composite coating keeps a higher microhardness of ~380 HV₁₀₀ (Fig. 1c3 and 2c).

Discussion

The above analysis indicates that the electrochemical processes were quite different for the traditional and sol-enhanced Ni–TiO₂ composite coatings. The orientation of coatings is mainly determined by grain growth. In electrochemical deposition, the microstructure of coatings is mainly controlled by overpotential. The detailed mechanisms are discussed below.

Grain growth during sol-enhanced electroplating process.—The effect of sol addition on the Ni electroplating can be analyzed from the XRD patterns in Fig. 7. The grain orientation of the traditional Ni coating was along [220] at the beginning of deposition (Fig. 7a). However, after the sol was added into the electrolyte, the relative intensity of the peak [220] decreased, indicating that the growth of Ni grains along [220] was slowed down. With the deposition process, the effect of TiO₂ sol on the Ni plating became larger, evidenced by the decreasing intensity of the [220] peak, as shown in Fig. 7b–d. Meanwhile, the peaks of [200] were almost unchanged. Obviously, the sol addition significantly affects the Ni grains growth.

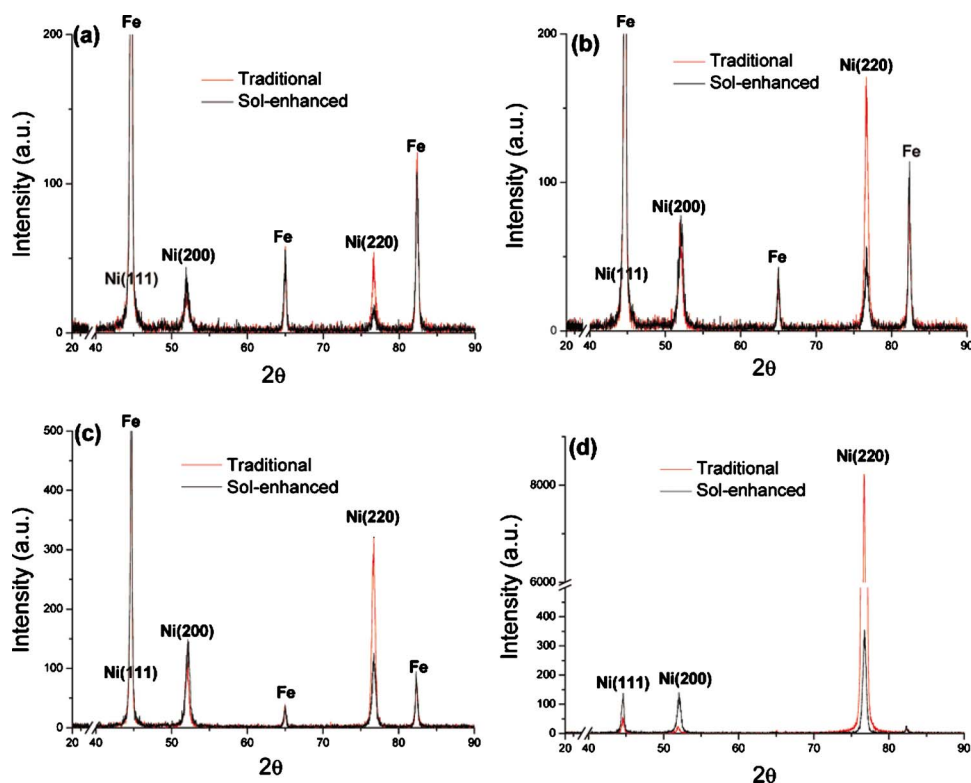


Figure 7. (Color online) XRD patterns of the traditional Ni coating (red lines) and the sol-enhanced Ni-TiO₂ composite coating (black lines) prepared at 50 mA cm⁻² for (a) 30 s, (b) 2 min, (c) 5 min, and (d) 10 min.

ing along [220]. As the surface energy determines the preferential growth direction, the addition of sol probably changes the surface energy of different planes.³⁰

Process of sol-enhanced electrodeposition.— Experimental results indicated that the mechanical properties of the sol-enhanced Ni-TiO₂ composite coatings were mainly determined by the highly dispersive TiO₂ nanoparticles.²⁸ The organic components in the TiO₂ sol mainly influenced the physical and chemical behaviors of the sol. Therefore, the electrochemical process of the sol-enhanced electrodeposition is discussed based on the effect of the TiO₂ nanoparticles.

The mechanism of the composite electrodeposition has been investigated since the 1960s,³¹⁻³⁵ and three main mechanisms were proposed^{4,35}: (i) electrophoretic movement of the positively charged particles to the cathode, (ii) adsorption of the particles at the electrode surface by van der Waals forces, and (iii) mechanical inclusion of the particles into the layer. According to the above mechanisms, it is proposed that two key factors in our present experiment, i.e., formation and movement of TiO₂ nanoparticles, should be emphasized to explain the sol-enhanced electrochemical process.

Formation of TiO₂ nanoparticles.— The formation of TiO₂ nanoparticles has been discussed in a previous paper.²⁸ As a summary, when a small amount of transparent sol solution was added into the conventional electroplating solution, the concentrated hydrate Ni ions in the solution destabilized the sol, leading to polymerization of TiO₂ sol. It was reported that the condensation process of Ti macromolecule ions started before the completion of hydrolysis in neutral and basic conditions, and the formation of an ordered structure was hindered.^{36,37} Thus, the amorphous TiO₂ nanoparticles formed in the electrolyte.

Once the nanoparticles formed in the electrolyte, some of them were immediately physically adsorbed onto the freshly deposited surface based on the Martin-Williams model.³² Some of them were immediately adsorbed by hydrate Ni ions due to their large surface areas based on the Whithers model.³¹ They were highly dispersed in the electrolyte, as schematically shown in Fig. 8a. The ethanol and DEA probably also contributed to the dispersion of the ion-adsorbed

TiO₂ nanoparticles. In contrast, for the solid powder mixing Ni-TiO₂ composite coatings, the nanoparticles were agglomerated up to several hundred nanometers when they were added into the electroplating solution, so the actual situation is that the Ni ions surrounded the large clusters of TiO₂ particles (Fig. 8b).

Movement of TiO₂ nanoparticles.— As discussed above, the TiO₂ nanoparticles existed in two forms during electroplating, i.e., physical adsorption onto the freshly deposited surface and hydrate Ni ion-adsorbed TiO₂ nanoparticles. We have previously described the formation of the sol-enhanced composite coatings partially under the control of physical adsorption of TiO₂ nanoparticles.²⁸ Here, we mainly analyze the influence of hydrate Ni ion-adsorbed TiO₂ nanoparticles.

The overall composite deposition process can be shown in five steps (Fig. 9a).⁴ These steps describe the process of particles from the solution to their incorporation in the metal matrix. The first stage postulates the formation of an electroactive ionic cloud surrounding the particles as soon as the particles are introduced into the electrolyte. Under the action of convection, these ionically enveloped particles are transported to the hydrodynamic boundary layer, migrate across the layer, and then are conveyed by diffusion to the cathode.

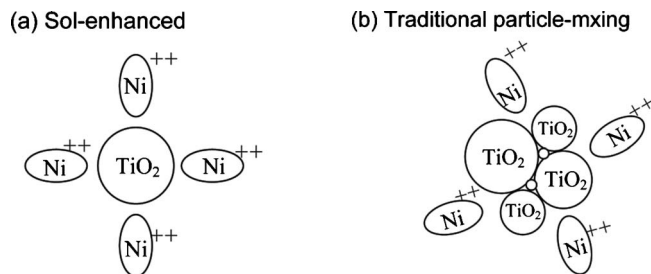


Figure 8. A schematic drawing to show the hydrate Ni ions and adsorbed TiO₂ particles: (a) The sol-enhanced and (b) the traditional particle-mixing electrodeposition process.

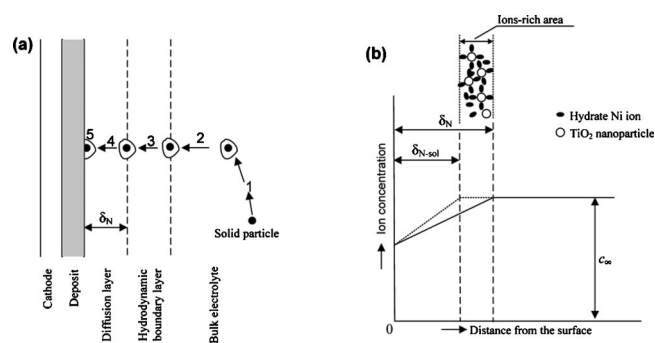


Figure 9. (a) Process steps in codeposition and incorporation of a solid particle into the deposit: (1) Formation of an ion cloud around the particle, (2) transport by means of convection, (3) transport by diffusion, (4) reduction reaction, and (5) adsorption. (b) The schematic diagram of the concentration-depth profile during the sol-enhanced electroplating.

After the ionic cloud is entirely or partly reduced, the particles are deposited and incorporated in the metal matrix as the metal ions are discharged, so “burying” the inert particles.

There are three main mechanisms involved in the delivery of ions to the cathode surface, i.e., migration (under a potential gradient), diffusion (under a concentration gradient), and convection (movement of the electrolyte solution itself). It is believed that the overall contribution to the supply of ions from the migration process is very small and can be neglected.⁴ The convection resulted from the movement of bulk solution is determined by stirring. Such movement of solution ceases to be significant in the diffusion layer, and movement of ions across the diffusion layer takes place by diffusion. The driving force for diffusion is the concentration gradient, more suitably expressed as the concentration polarization. According to the electrochemical theory, there are two important polarizations in the electroplating process: electrochemical (activation) polarization and concentration polarization. Concentration polarization can be increased by reducing the thickness of the diffusion layer. There exists a limited current density (i_L), which is determined by concentration polarization, expressed as

$$i_L = zFD \frac{c_\infty}{\delta_N} \quad [2]$$

where z is the number of electrons per ion being transferred, F is Faraday’s constant, c_∞ is the ion concentration in bulk solution, and δ_N is the thickness of the diffusion layer. When the current is below i_L , the electroplating process is controlled by electrochemical polarization; otherwise, the process is controlled by concentration polarization. In the latter case, metal ions tend to discharge preferentially at the tips of the protrusions, and the nucleus is difficult to grow, which tends to result in the formation of a loose and dendritic surface.

Figure 9b shows a schematic diagram of the concentration-depth profile during the sol-enhanced electroplating. During the deposition process, a large amount of hydrate Ni ions was adsorbed on the surface of the newly formed TiO₂ nanoparticles due to the large surface areas of the nanosized particles. The ion-adsorbed nanoparticles were conveyed to the diffusion layer under the effect of stirring. An ion-rich area formed at the edge of the diffusion layer (Fig. 9b), where the ion concentration was so large that it reached the concentration (c_∞) of the bulk electrolyte. In this case, the thickness of the diffusion layer decreased from δ_N to δ_{N-sol} , leading to the increase in the limited current density (i_L). Therefore, the critical current density to form the dendritic surface increased during the sol-enhanced deposition process.

In contrast, during the traditional composite coating process, because of poor adsorption of hydrous Ni²⁺ onto the surface of the agglomerated TiO₂ particles, the thickness of the diffusion layer and

the limited current density i_L did not change significantly. Therefore, at 100 mA cm⁻², the concentration polarization controlled the electrochemical process, leading to the formation of a loose and dendritic structure (Fig. 1b3 and 2a and b). The process of sol-enhanced electroplating was controlled by electrochemical polarization, resulting in a compact structure, as seen in Fig. 1c3 and 2c.

The experimental confirmation of the above-described mechanism is needed and now in progress. We are now designing an electrochemical microsetup to investigate the effect of sol addition on the diffusion layer, activation energy, nucleation, and grain growth. The process seems complex based on some preliminary experimental results. In the present paper, the comparison of structures and properties between the traditional and sol-enhanced Ni–TiO₂ composite films was emphasized; therefore, the discussions were mainly based on the above differences. Soon, the detailed mechanism for the sol-enhanced composite plating will be presented based on electrochemical polarization theory and TEM observation.

Conclusions

A Ni–TiO₂ composite film has been prepared by sol-enhanced electroplating. In this process, a small amount of transparent TiO₂ sol was added into the traditional electroplating Ni solution, forming highly dispersive TiO₂ nanoparticles, which codeposited with Ni to form a nanocomposite coating. The in situ formation of fine TiO₂ nanoparticles originating from sol changed the electrochemical behavior and polarization mechanism, avoiding the loose and dendritic surface structure at higher current deposition. The highly dispersive nanoparticles and the dense structure led to the significant improvement in mechanical properties of Ni–TiO₂ composite coatings prepared at a high current density.

Acknowledgments

The project is partially funded by New Zealand FRST IIOF grant UoA 0601 and an Auckland UniServices grant. We thank the technical staff in the Department of Chemical and Materials Engineering and Research Centre for Surface and Materials Science for assistance.

The University of Auckland assisted in meeting the publication costs of this article.

References

- O. P. Watts, *Trans. Am. Electrochem. Soc.*, **29**, 395 (1916).
- G. A. Di Bari, in *Morden Electroplating*, 4th ed., M. Schlesinger and M. Paunovic, Editors, p. 139, John Wiley & Sons, New York (2000).
- S. Field and A. D. Weill, *Electro-Plating*, 2nd ed., p. 136, Sir Isaac Pitman & Sons, London (1935).
- N. Kanani, *Electroplating: Basic Principles, Processes and Practice*, Elsevier Advanced Technology, Oxford (2004).
- J. Sadowski-Mazur, M. E. Warwick, and R. Walker, *Trans. Inst. Met. Finish.*, **64**, 142 (1976).
- V. Sova and H. Bollhalder, *Plat. Surf. Finish.*, **75**, 53 (1988).
- J. Zahavi and J. Hazan, *Plat. Surf. Finish.*, **70**, 57 (1983).
- S. S. Tulsi, *Trans. Inst. Met. Finish.*, **61**, 147 (1983).
- P. R. Ebdon, *Plat. Surf. Finish.*, **75**, 65 (1988).
- R. R. Oberle, M. R. Scanlon, R. C. Cammarata, and P. C. Searson, *Appl. Phys. Lett.*, **66**, 19 (1995).
- I. Shao, P. M. Vereecken, R. C. Cammarata, and P. C. Searson, *J. Electrochem. Soc.*, **149**, C610 (2002).
- K. C. Chan, C. L. Wang, K. F. Zhang, and G. Pang, *Scr. Mater.*, **51**, 605 (2004).
- W. Wang, F. Y. Hou, H. Wang, and H. T. Guo, *Scr. Mater.*, **53**, 613 (2005).
- B. S. Xu, H. D. Wang, S. Y. Dong, B. Jiang, and W. Y. Tu, *Electrochem. Commun.*, **7**, 572 (2005).
- E. Orowan, in *Symposium on Internal Stresses in Metals and Alloys*, Institute of Metals, p. 451 (1948).
- M. F. Ashby, in *Physics of Strength and Plasticity*, A. S. Argon, Editor, p. 113, MIT Press, Cambridge, MA (1969).
- J. R. Vinson and T. W. Chou, *Composite Materials and Their Use in Structures*, p. 124, Applied Science, London (1975).
- S. Dobatkin and X. Sauvage, in *Bulk Nanostructured Materials*, M. J. Zehetbauer and Y. T. Zhu, Editors, p. 595, Wiley-VCH Verlag GmbH, Weinheim (2009).
- W. Stöber, A. Fink, and E. Bohn, *J. Colloid Interface Sci.*, **26**, 62 (1968).
- J. Livage, *Bull. Mater. Sci.*, **22**, 201 (1999).
- M. J. Iqbal and M. N. Ashiq, *Scr. Mater.*, **56**, 145 (2007).
- Q. L. Zhang, F. Wu, H. Yang, and D. Zou, *J. Mater. Chem.*, **18**, 5339 (2008).
- A. E. Gash, T. M. Tillotson, J. H. Satcher, J. F. Poco, L. W. Hrubesh, and R. L. Simpson, *Chem. Mater.*, **13**, 999 (2001).

24. C. N. Chervin, B. J. Clapsaddle, H. W. Chiu, A. E. Gash, J. H. Satcher, Jr., and S. M. Kauzlarich, *Chem. Mater.*, **18**, 4865 (2006).
25. M. Kallala, C. Sanchez, and B. Cabane, *Phys. Rev. E*, **48**, 3692 (1993).
26. T. Ogihara, M. Ikeda, M. Kato, and N. Mizutani, *J. Am. Ceram. Soc.*, **72**, 1598 (1989).
27. W. W. Chen and W. Gao, Provisional Pat. NZ578038, New Zealand (2009).
28. W. W. Chen, Y. D. He, and W. Gao, *Surf. Coat. Technol.*, **204**, 2487 (2010).
29. J. J. Qiu, Z. G. Jin, Z. F. Liu, X. X. Liu, G. Q. Liu, W. B. Wu, X. Zhang, and X. D. Gao, *Thin Solid Films*, **515**, 2897 (2007).
30. T. Watanabe, *Nano-plating: Microstructure Control Theory of Plated Film and Database of Plated Film Microstructure*, Elsevier, Amsterdam (2004).
31. J. C. Withers, *Prod. Finish.*, **26**, 62 (1962).
32. R. V. Williams and P. W. Martin, *Trans. Inst. Met. Finish.*, **42**, 182 (1964).
33. E. A. Brandes and D. Goldthorpe, *Metalurgia (Bucharest)*, **76**, 195 (1967).
34. J. P. Celis, J. R. Roos, C. Buelens, and J. Fransaeer, *Trans. Inst. Met. Finish.*, **69**, 133 (1991).
35. A. Hovestad and L. J. J. Janssen, *J. Appl. Electrochem.*, **25**, 519 (1995).
36. M. Gopal, W. J. Mobery Chan, and L. C. De Jonghe, *J. Mater. Sci.*, **32**, 6001 (1997).
37. Z. L. Tang, J. Y. Zhang, Z. Cheng, and Z. T. Zhang, *Mater. Chem. Phys.*, **77**, 314 (2003).